

Study of $\phi \rightarrow K\bar{K}$ and $K_S^0 - K_L^0$ asymmetry in the amplitude analysis of $D_s^+ \rightarrow K_S^0 K_L^0 \pi^+$ decay

- M. Ablikim¹, M. N. Achasov^{4,c}, P. Adlarson⁷⁷, X. C. Ai⁸², R. Aliberti³⁶, A. Amoroso^{76A,76C}, Q. An^{73,59,a}, Y. Bai⁵⁸, O. Bakina³⁷, Y. Ban^{47,h}, H.-R. Bao⁶⁵, V. Batozskaya^{1,45}, K. Begzsuren³³, N. Berger³⁶, M. Berlowski⁴⁵, M. Bertani^{29A}, D. Bettom^{30A}, F. Bianchi^{76A,76C}, E. Bianco^{76A,76C}, A. Bortone^{76A,76C}, I. Boyko³⁷, R. A. Briere⁵, A. Brueggemann⁷⁰, H. Cai⁷⁸, M. H. Cai^{39,k,l}, X. Cai^{1,59}, A. Calcaterra^{29A}, G. F. Cao^{1,65}, N. Cao^{1,65}, S. A. Cetin^{63A}, X. Y. Chai^{47,h}, J. F. Chang^{1,59}, G. R. Che⁴⁴, Y. Z. Che^{1,59,65}, G. Chelkov^{37,b}, C. H. Chen⁹, Chao Chen⁵⁶, G. Chen¹, H. S. Chen^{1,65}, H. Y. Chen²¹, M. L. Chen^{1,59,65}, S. J. Chen⁴³, S. L. Chen⁴⁶, S. M. Chen⁶², T. Chen^{1,65}, X. R. Chen^{32,65}, X. T. Chen^{1,65}, X. Y. Chen^{12,g}, Y. B. Chen^{1,59}, Y. Q. Chen³⁵, Y. Q. Chen¹⁶, Z. J. Chen^{26,i}, Z. K. Chen⁶⁰, S. K. Choi¹⁰, X. Chu^{12,g}, G. Cibinetto^{30A}, F. Cossio^{76C}, J. Cottee-Meldrum⁶⁴, J. J. Cui⁵¹, H. L. Dai^{1,59}, J. P. Dai⁸⁰, A. Dbeysi¹⁹, R. E. de Boer³, D. Dedovich³⁷, C. Q. Deng⁷⁴, Z. Y. Deng¹, A. Denig³⁶, I. Denysenko³⁷, M. Destefanis^{76A,76C}, F. De Mori^{76A,76C}, B. Ding^{68,1}, X. X. Ding^{47,h}, Y. Ding⁴¹, Y. Ding³⁵, Y. X. Ding³¹, J. Dong^{1,59}, L. Y. Dong^{1,65}, M. Y. Dong^{1,59,65}, X. Dong⁷⁸, M. C. Du¹, S. X. Du⁸², S. X. Du^{12,g}, Y. Y. Duan⁵⁶, Z. H. Duan⁴³, P. Egorov^{37,b}, G. F. Fan⁴³, J. J. Fan²⁰, Y. H. Fan⁴⁶, J. Fang^{1,59}, J. Fang⁶⁰, S. S. Fang^{1,65}, W. X. Fang¹, Y. Q. Fang^{1,59}, R. Farinelli^{30A}, L. Fava^{76B,76C}, F. Feldbauer³, G. Felici^{29A}, C. Q. Feng^{73,59}, J. H. Feng¹⁶, L. Feng^{39,k,l}, Q. X. Feng^{39,k,l}, Y. T. Feng^{73,59}, M. Fritsch³, C. D. Fu¹, J. L. Fu⁶⁵, Y. W. Fu^{1,65}, H. Gao⁶⁵, X. B. Gao⁴², Y. N. Gao²⁰, Y. N. Gao^{47,h}, Y. Y. Gao³¹, Yang Gao^{73,59}, S. Garbolino^{76C}, I. Garzia^{30A,30B}, P. T. Ge²⁰, Z. W. Ge⁴³, C. Geng⁶⁰, E. M. Gersabeck⁶⁹, A. Gilman⁷¹, K. Goetzen¹³, J. D. Gong³⁵, L. Gong⁴¹, W. X. Gong^{1,59}, W. Gradl³⁶, S. Gramigna^{30A,30B}, M. Greco^{76A,76C}, M. H. Gu^{1,59}, Y. T. Gu¹⁵, C. Y. Guan^{1,65}, A. Q. Guo³², L. B. Guo⁴², M. J. Guo⁵¹, R. P. Guo⁵⁰, Y. P. Guo^{12,g}, A. Guskov^{37,b}, J. Gutierrez²⁸, K. L. Han⁶⁵, T. T. Han¹, F. Hanisch³, K. D. Hao^{73,59}, X. Q. Hao²⁰, F. A. Harris⁶⁷, K. K. He⁵⁶, K. L. He^{1,65}, F. H. Heinsius³, C. H. Heinz³⁶, Y. K. Heng^{1,59,65}, C. Herold⁶¹, T. Holtmann³, P. C. Hong³⁵, G. Y. Hou^{1,65}, X. T. Hou^{1,65}, Y. R. Hou⁶⁵, Z. L. Hou¹, H. M. Hu^{1,65}, J. F. Hu^{57,j}, Q. P. Hu^{73,59}, S. L. Hu^{12,g}, T. Hu^{1,59,65}, Y. Hu¹, Z. M. Hu⁶⁰, G. S. Huang^{73,59}, K. X. Huang⁶⁰, L. Q. Huang^{32,65}, P. Huang⁴³, X. T. Huang⁵¹, Y. P. Huang¹, Y. S. Huang⁶⁰, T. Hussain⁷⁵, N. Hüskens³⁶, N. in der Wiesche⁷⁰, J. Jackson²⁸, S. Janchiv³³, Q. Ji¹, Q. P. Ji²⁰, W. Ji^{1,65}, X. B. Ji^{1,65}, X. L. Ji^{1,59}, Y. Y. Ji⁵¹, Z. K. Jia^{73,59}, D. Jiang^{1,65}, H. B. Jiang⁷⁸, P. C. Jiang^{47,h}, S. J. Jiang⁹, T. J. Jiang¹⁷, X. S. Jiang^{1,59,65}, Y. Jiang⁶⁵, J. B. Jiao⁵¹, J. K. Jiao³⁵, Z. Jiao²⁴, S. Jin⁴³, Y. Jin⁶⁸, M. Q. Jing^{1,65}, X. M. Jing⁶⁵, T. Johansson⁷⁷, S. Kabana³⁴, N. Kalantar-Nayestanaki⁶⁶, X. L. Kang⁹, X. S. Kang⁴¹, M. Kavatsyuk⁶⁶, B. C. Ke⁸², V. Khachatryan²⁸, A. Khouakz⁷⁰, R. Kiuchi¹, O. B. Kolcu^{63A}, B. Kopf³, M. Kuessner³, X. Kui^{1,65}, N. Kumar²⁷, A. Kupsc^{45,77}, W. Kuihn³⁸, Q. Lan⁷⁴, W. N. Lan²⁰, T. T. Lei^{73,59}, M. Lellmann³⁶, T. Lenz³⁶, C. Li⁴⁸, C. Li⁴⁴, C. H. Li⁴⁰, C. K. Li²¹, Cheng Li^{73,59}, D. M. Li⁸², F. Li^{1,59}, G. Li¹, H. B. Li^{1,65}, H. J. Li²⁰, H. N. Li^{57,j}, Hui Li⁴⁴, J. R. Li⁶², J. S. Li⁶⁰, K. Li¹, K. L. Li^{39,k,l}, K. L. Li²⁰, L. J. Li^{1,65}, Lei Li⁴⁹, M. H. Li⁴⁴, M. R. Li^{1,65}, P. L. Li⁶⁵, P. R. Li^{39,k,l}, Q. M. Li^{1,65}, Q. X. Li⁵¹, R. Li^{18,32}, S. X. Li¹², T. Li⁵¹, T. Y. Li⁴⁴, W. D. Li^{1,65}, W. G. Li^{1,a}, X. Li^{1,65}, X. H. Li^{73,59}, X. L. Li⁵¹, X. Y. Li^{1,8}, X. Z. Li⁶⁰, Y. Li²⁰, Y. G. Li^{47,h}, Y. P. Li³⁵, Z. J. Li⁶⁰, Z. Y. Li⁸⁰, C. Liang⁴³, H. Liang^{73,59}, Y. F. Liang⁵⁵, Y. T. Liang^{32,65}, G. R. Liao¹⁴, L. B. Liao⁶⁰, M. H. Liao⁶⁰, Y. P. Liao^{1,65}, J. Libby²⁷, A. Limphirat⁶¹, C. C. Lin⁵⁶, C. X. Lin⁶⁵, D. X. Lin^{32,65}, L. Q. Lin⁴⁰, T. Lin¹, B. J. Liu¹, B. X. Liu⁷⁸, C. Liu³⁵, C. X. Liu¹, F. Liu¹, F. H. Liu⁵⁴, Feng Liu⁶, G. M. Liu^{57,j}, H. Liu^{39,k,l}, H. B. Liu¹⁵, H. H. Liu¹, H. M. Liu^{1,65}, Huihui Liu²², J. B. Liu^{73,59}, J. J. Liu²¹, K. Liu^{39,k,l}, K. Liu⁷⁴, K. Y. Liu⁴¹, Ke Liu²³, L. Liu^{73,59}, L. C. Liu⁴⁴, Lu Liu⁴⁴, M. H. Liu^{12,g}, P. L. Liu¹, Q. Liu⁶⁵, S. B. Liu^{73,59}, T. Liu^{12,g}, W. K. Liu⁴⁴, W. M. Liu^{73,59}, W. T. Liu⁴⁰, X. Liu^{39,k,l}, X. Liu⁴⁰, X. K. Liu^{39,k,l}, X. Y. Liu⁷⁸, Y. Liu^{39,k,l}, Y. Liu⁸², Y. B. Liu⁴⁴, Z. A. Liu^{1,59,65}, Z. D. Liu⁹, Z. Q. Liu⁵¹, X. C. Lou^{1,59,65}, F. X. Lu⁶⁰, H. J. Lu²⁴, J. G. Lu^{1,59}, X. L. Lu¹⁶, Y. Lu⁷, Y. H. Lu^{1,65}, Y. P. Lu^{1,59}, Z. H. Lu^{1,65}, C. L. Luo⁴², J. R. Luo⁶⁰, J. S. Luo^{1,65}, M. X. Luo⁸¹, T. Luo^{12,g}, X. L. Luo^{1,59}, Z. Y. Lv²³, X. R. Lyu^{65,p}, Y. F. Lyu⁴⁴, Y. H. Lyu⁸², F. C. Ma⁴¹, H. Ma⁸⁰, H. L. Ma¹, J. L. Ma^{1,65}, L. L. Ma⁵¹, L. R. Ma⁶⁸, Q. M. Ma¹, R. Q. Ma^{1,65}, R. Y. Ma²⁰, T. Ma^{73,59}, X. T. Ma^{1,65}, X. Y. Ma^{1,59}, Y. M. Ma³², F. E. Maas¹⁹, I. MacKay⁷¹, M. Maggiore^{76A,76C}, S. Malde⁷¹, H. X. Mao^{47,h}, Z. P. Mao¹, S. Marcello^{76A,76C}, A. Marshall⁶⁴, F. M. Melendi^{30A,30B}, Y. H. Meng⁶⁵, Z. X. Meng⁶⁸, J. G. Messchendorp^{13,66}, G. Mezzadri^{30A}, H. Miao^{1,65}, T. J. Min⁴³, R. E. Mitchell²⁸, X. H. Mo^{1,59,65}, B. Moses²⁸, N. Yu. Muchnoi^{4,c}, J. Muskalla³⁶, Y. Nefedov³⁷, F. Nerling^{19,e}, L. S. Nie²¹, I. B. Nikolaev^{4,c}, Z. Ning^{1,59}, S. Nisar^{11,m}, Q. L. Niu^{39,k,l}, W. D. Niu^{12,g}, C. Normand⁶⁴, S. L. Olsen^{10,65}, Q. Ouyang^{1,59,65}, S. Pacetti^{29B,29C}, X. Pan⁵⁶, Y. Pan⁵⁸, A. Pathak¹⁰, Y. P. Pei^{73,59}, M. Pelizaeus³, H. P. Peng^{73,59}, X. J. Peng^{39,k,l}, Y. Y. Peng^{39,k,l}, K. Peters^{13,e}, K. Petridis⁶⁴, J. L. Ping⁴², R. G. Ping^{1,65}, S. Plura³⁶, V. Prasad³⁴, F. Z. Qi¹, H. R. Qi⁶², M. Qi⁴³, S. Qian^{1,59}, W. B. Qian⁶⁵, C. F. Qiao⁶⁵, J. H. Qiao²⁰, J. J. Qin⁷⁴, J. L. Qin⁵⁶, L. Q. Qin¹⁴, L. Y. Qin^{73,59}, P. B. Qin⁷⁴, X. P. Qin^{12,g}, X. S. Qin⁵¹, Z. H. Qin^{1,59}, J. F. Qin¹, Z. H. Qu⁷⁴, J. Rademacker⁶⁴, C. F. Redmer³⁶, A. Rivetti^{76C}, M. Rolando^{76C}, G. Rong^{1,65}, S. S. Rong^{1,65}, F. Rosini^{29B,29C}, Ch. Rosner¹⁹, M. Q. Ruan^{1,59}, N. Salone⁴⁵, A. Sarantsev^{37,d}, Y. Schelhaas³⁶, K. Schoenning⁷⁷, M. Scodellaggio^{30A}, K. Y. Shan^{12,g}, W. Shan²⁵, X. Y. Shan^{73,59}, Z. J. Shang^{39,k,l}, J. F. Shangguan¹⁷, L. G. Shao^{1,65}, M. Shao^{73,59}, C. P. Shen^{12,g}, H. F. Shen^{1,8}, W. H. Shen⁶⁵, X. Y. Shen^{1,65}, B. A. Shi⁶⁵, H. Shi^{73,59}, J. L. Shi^{12,g}, J. Y. Shi¹, S. Y. Shi⁷⁴, X. Shi^{1,59}, H. L. Song^{73,59}, J. J. Song²⁰, T. Z. Song⁶⁰, W. M. Song³⁵, Y. J. Song^{12,g}, Y. X. Song^{47,h,n}, S. Sosio^{76A,76C}, S. Spataro^{76A,76C}, F. Stieler³⁶, S. S. Su⁴¹, Y. J. Su⁶⁵, G. B. Sun⁷⁸, G. X. Sun¹, H. Sun⁶⁵, H. K. Sun¹, J. F. Sun²⁰, K. Sun⁶², L. Sun⁷⁸, S. S. Sun^{1,65}, T. Sun^{52,f}, Y. C. Sun⁷⁸, Y. H. Sun³¹, Y. J. Sun^{73,59}, Y. Z. Sun¹, Z. Q. Sun^{1,65}, Z. T. Sun⁵¹, C. J. Tang⁵⁵, G. Y. Tang¹, J. Tang⁶⁰, J. J. Tang^{73,59}, L. F. Tang⁴⁰, Y. A. Tang⁷⁸, L. Y. Tao⁷⁴, M. Tat⁷¹, J. X. Teng^{73,59}, J. Y. Tian^{73,59}, W. H. Tian⁶⁰, Y. Tian³², Z. F. Tian⁷⁸, I. Uman^{63B}, B. Wang⁶⁰, B. Wang¹, Bo Wang^{73,59}, C. Wang^{39,k,l}, C. Wang²⁰, Cong Wang²³, D. Y. Wang^{47,h}, H. J. Wang^{39,k,l}, J. J. Wang⁷⁸, K. Wang^{1,59}, L. L. Wang¹, L. W. Wang³⁵, M. Wang⁵¹, M. Wang^{73,59}, N. Y. Wang⁶⁵, S. Wang^{12,g}, T. Wang^{12,g}, T. J. Wang⁴⁴, W. Wang⁶⁰, W. Wang⁷⁴, W. P. Wang^{36,59,73,o}, X. Wang^{47,h}, X. F. Wang^{39,k,l}, X. J. Wang⁴⁰, X. L. Wang^{12,g}, X. N. Wang¹, Y. Wang⁶², Y. D. Wang⁴⁶, Y. F. Wang^{1,59,65}, Y. H. Wang^{39,k,l}, Y. L. Wang²⁰,

Y. N. Wang⁷⁸, Y. Q. Wang¹, Yaqian Wang¹⁸, Yi Wang⁶², Yuan Wang^{18,32}, Z. Wang^{1,59}, Z. L. Wang², Z. L. Wang⁷⁴,
 Z. Q. Wang^{12,g}, Z. Y. Wang^{1,65}, D. H. Wei¹⁴, H. R. Wei⁴⁴, F. Weidner⁷⁰, S. P. Wen¹, Y. R. Wen⁴⁰, U. Wiedner³,
 G. Wilkinson⁷¹, M. Wolke⁷⁷, C. Wu⁴⁰, J. F. Wu^{1,8}, L. H. Wu¹, L. J. Wu^{1,65}, L. J. Wu²⁰, Lianjie Wu²⁰, S. G. Wu^{1,65},
 S. M. Wu⁶⁵, X. Wu^{12,g}, X. H. Wu³⁵, Y. J. Wu³², Z. Wu^{1,59}, L. Xia^{73,59}, X. M. Xian⁴⁰, B. H. Xiang^{1,65}, D. Xiao^{39,k,l},
 G. Y. Xiao⁴³, H. Xiao⁷⁴, Y. L. Xiao^{12,g}, Z. J. Xiao⁴², C. Xie⁴³, K. J. Xie^{1,65}, X. H. Xie^{47,h}, Y. Xie⁵¹, Y. G. Xie^{1,59},
 Y. H. Xie⁶, Z. P. Xie^{73,59}, T. Y. Xing^{1,65}, C. F. Xu^{1,65}, C. J. Xu⁶⁰, G. F. Xu¹, H. Y. Xu^{68,2}, H. Y. Xu², M. Xu^{73,59},
 Q. J. Xu¹⁷, Q. N. Xu³¹, T. D. Xu⁷⁴, W. Xu¹, W. L. Xu⁶⁸, X. P. Xu⁵⁶, Y. Xu^{12,g}, Y. Xu⁴¹, Y. C. Xu⁷⁹, Z. S. Xu⁶⁵, F. Yan^{12,g},
 H. Y. Yan⁴⁰, L. Yan^{12,g}, W. B. Yan^{73,59}, W. C. Yan⁸², W. H. Yan⁶, W. P. Yan²⁰, X. Q. Yan^{1,65}, H. J. Yang^{52,f}, H. L. Yang³⁵,
 H. X. Yang¹, J. H. Yang⁴³, R. J. Yang²⁰, T. Yang¹, Y. Yang^{12,g}, Y. F. Yang⁴⁴, Y. H. Yang⁴³, Y. Q. Yang⁹, Y. X. Yang^{1,65},
 Y. Z. Yang²⁰, M. Ye^{1,59}, M. H. Ye⁸, Z. J. Ye^{57,j}, Junhao Yin⁴⁴, Z. Y. You⁶⁰, B. X. Yu^{1,59,65}, C. X. Yu⁴⁴, G. Yu¹³, J. S. Yu^{26,i},
 M. C. Yu⁴¹, T. Yu⁷⁴, X. D. Yu^{47,h}, Y. C. Yu⁸², C. Z. Yuan^{1,65}, H. Yuan^{1,65}, J. Yuan⁴⁶, J. Yuan³⁵, L. Yuan², S. C. Yuan^{1,65},
 X. Q. Yuan¹, Y. Yuan^{1,65}, Z. Y. Yuan⁶⁰, C. X. Yue⁴⁰, Ying Yue²⁰, A. A. Zafar⁷⁵, S. H. Zeng^{64A,64B,64C,64D}, X. Zeng^{12,g},
 Y. Zeng^{26,i}, Y. J. Zeng^{1,65}, Y. J. Zeng⁶⁰, X. Y. Zhai³⁵, Y. H. Zhan⁶⁰, A. Q. Zhang^{1,65}, B. L. Zhang^{1,65}, B. X. Zhang¹,
 D. H. Zhang⁴⁴, G. Y. Zhang^{1,65}, G. Y. Zhang²⁰, H. Zhang⁸², H. Zhang^{73,59}, H. C. Zhang^{1,59,65}, H. H. Zhang⁶⁰,
 H. Q. Zhang^{1,59,65}, H. R. Zhang^{73,59}, H. Y. Zhang^{1,59}, J. Zhang⁸², J. Zhang⁶⁰, J. J. Zhang⁵³, J. L. Zhang²¹, J. Q. Zhang⁴²,
 J. S. Zhang^{12,g}, J. W. Zhang^{1,59,65}, J. X. Zhang^{39,k,l}, J. Y. Zhang¹, J. Z. Zhang^{1,65}, Jianyu Zhang⁶⁵, L. M. Zhang⁶²,
 Lei Zhang⁴³, N. Zhang⁸², P. Zhang^{1,65}, Q. Zhang²⁰, Q. Y. Zhang³⁵, R. Y. Zhang^{39,k,l}, S. H. Zhang^{1,65}, Shulei Zhang^{26,i},
 X. M. Zhang¹, X. Y. Zhang⁴¹, X. Y. Zhang⁵¹, Y. Zhang¹, Y. Zhang⁷⁴, Y. T. Zhang⁸², Y. H. Zhang^{1,59}, Y. M. Zhang⁴⁰,
 Z. D. Zhang¹, Z. H. Zhang¹, Z. L. Zhang³⁵, Z. L. Zhang⁵⁶, Z. X. Zhang²⁰, Z. Y. Zhang⁴⁴, Z. Y. Zhang⁷⁸, Z. Z. Zhang⁴⁶,
 Zh. Zh. Zhang²⁰, G. Zhao¹, J. Y. Zhao^{1,65}, J. Z. Zhao^{1,59}, L. Zhao¹, Lei Zhao^{73,59}, M. G. Zhao⁴⁴, N. Zhao⁸⁰, R. P. Zhao⁶⁵,
 S. J. Zhao⁸², Y. B. Zhao^{1,59}, Y. L. Zhao⁵⁶, Y. X. Zhao^{32,65}, Z. G. Zhao^{73,59}, A. Zhemchugov^{37,b}, B. Zheng⁷⁴, B. M. Zheng³⁵,
 J. P. Zheng^{1,59}, W. J. Zheng^{1,65}, X. R. Zheng²⁰, Y. H. Zheng^{65,p}, B. Zhong⁴², C. Zhong²⁰, H. Zhou^{36,51,o}, J. Q. Zhou³⁵,
 J. Y. Zhou³⁵, S. Zhou⁶, X. Zhou⁷⁸, X. K. Zhou⁶, X. R. Zhou^{73,59}, X. Y. Zhou⁴⁰, Y. X. Zhou⁷⁹, Y. Z. Zhou^{12,g}, A. N. Zhu⁶⁵,
 J. Zhu⁴⁴, K. Zhu¹, K. J. Zhu^{1,59,65}, K. S. Zhu^{12,g}, L. Zhu³⁵, L. X. Zhu⁶⁵, S. H. Zhu⁷², T. J. Zhu^{12,g}, W. D. Zhu⁴²,
 W. D. Zhu^{12,g}, W. J. Zhu¹, W. Z. Zhu²⁰, Y. C. Zhu^{73,59}, Z. A. Zhu^{1,65}, X. Y. Zhuang⁴⁴, J. H. Zou¹, J. Zu^{73,59}

(BESIII Collaboration)

¹ Institute of High Energy Physics, Beijing 100049, People's Republic of China

² Beihang University, Beijing 100191, People's Republic of China

³ Bochum Ruhr-University, D-44780 Bochum, Germany

⁴ Budker Institute of Nuclear Physics SB RAS (BINP), Novosibirsk 630090, Russia

⁵ Carnegie Mellon University, Pittsburgh, Pennsylvania 15213, USA

⁶ Central China Normal University, Wuhan 430079, People's Republic of China

⁷ Central South University, Changsha 410083, People's Republic of China

⁸ China Center of Advanced Science and Technology, Beijing 100190, People's Republic of China

⁹ China University of Geosciences, Wuhan 430074, People's Republic of China

¹⁰ Chung-Ang University, Seoul, 06974, Republic of Korea

¹¹ COMSATS University Islamabad, Lahore Campus, Defence Road, Off Raiwind Road, 54000 Lahore, Pakistan

¹² Fudan University, Shanghai 200433, People's Republic of China

¹³ GSI Helmholtzcentre for Heavy Ion Research GmbH, D-64291 Darmstadt, Germany

¹⁴ Guangxi Normal University, Guilin 541004, People's Republic of China

¹⁵ Guangxi University, Nanning 530004, People's Republic of China

¹⁶ Guangxi University of Science and Technology, Liuzhou 545006, People's Republic of China

¹⁷ Hangzhou Normal University, Hangzhou 310036, People's Republic of China

¹⁸ Hebei University, Baoding 071002, People's Republic of China

¹⁹ Helmholtz Institute Mainz, Staudinger Weg 18, D-55099 Mainz, Germany

²⁰ Henan Normal University, Xinxiang 453007, People's Republic of China

²¹ Henan University, Kaifeng 475004, People's Republic of China

²² Henan University of Science and Technology, Luoyang 471003, People's Republic of China

²³ Henan University of Technology, Zhengzhou 450001, People's Republic of China

²⁴ Huangshan College, Huangshan 245000, People's Republic of China

²⁵ Hunan Normal University, Changsha 410081, People's Republic of China

²⁶ Hunan University, Changsha 410082, People's Republic of China

²⁷ Indian Institute of Technology Madras, Chennai 600036, India

²⁸ Indiana University, Bloomington, Indiana 47405, USA

²⁹ INFN Laboratori Nazionali di Frascati, (A)INFN Laboratori Nazionali di Frascati, I-00044, Frascati, Italy; (B)INFN Sezione di Perugia, I-06100, Perugia, Italy; (C)University of Perugia, I-06100, Perugia, Italy

³⁰ INFN Sezione di Ferrara, (A)INFN Sezione di Ferrara, I-44122, Ferrara, Italy; (B)University of Ferrara, I-44122, Ferrara, Italy

³¹ Inner Mongolia University, Hohhot 010021, People's Republic of China

³² Institute of Modern Physics, Lanzhou 730000, People's Republic of China

³³ Institute of Physics and Technology, Mongolian Academy of Sciences, Peace Avenue 54B, Ulaanbaatar 13330, Mongolia

³⁴ Instituto de Alta Investigación, Universidad de Tarapacá, Casilla 7D, Arica 1000000, Chile

- ³⁵ Jilin University, Changchun 130012, People's Republic of China
³⁶ Johannes Gutenberg University of Mainz, Johann-Joachim-Becher-Weg 45, D-55099 Mainz, Germany
³⁷ Joint Institute for Nuclear Research, 141980 Dubna, Moscow region, Russia
³⁸ Justus-Liebig-Universitaet Giessen, II. Physikalisches Institut, Heinrich-Buff-Ring 16, D-35392 Giessen, Germany
³⁹ Lanzhou University, Lanzhou 730000, People's Republic of China
⁴⁰ Liaoning Normal University, Dalian 116029, People's Republic of China
⁴¹ Liaoning University, Shenyang 110036, People's Republic of China
⁴² Nanjing Normal University, Nanjing 210023, People's Republic of China
⁴³ Nanjing University, Nanjing 210093, People's Republic of China
⁴⁴ Nankai University, Tianjin 300071, People's Republic of China
⁴⁵ National Centre for Nuclear Research, Warsaw 02-093, Poland
⁴⁶ North China Electric Power University, Beijing 102206, People's Republic of China
⁴⁷ Peking University, Beijing 100871, People's Republic of China
⁴⁸ Qufu Normal University, Qufu 273165, People's Republic of China
⁴⁹ Renmin University of China, Beijing 100872, People's Republic of China
⁵⁰ Shandong Normal University, Jinan 250014, People's Republic of China
⁵¹ Shandong University, Jinan 250100, People's Republic of China
⁵² Shanghai Jiao Tong University, Shanghai 200240, People's Republic of China
⁵³ Shanxi Normal University, Linfen 041004, People's Republic of China
⁵⁴ Shanxi University, Taiyuan 030006, People's Republic of China
⁵⁵ Sichuan University, Chengdu 610064, People's Republic of China
⁵⁶ Soochow University, Suzhou 215006, People's Republic of China
⁵⁷ South China Normal University, Guangzhou 510006, People's Republic of China
⁵⁸ Southeast University, Nanjing 211100, People's Republic of China
⁵⁹ State Key Laboratory of Particle Detection and Electronics, Beijing 100049, Hefei 230026, People's Republic of China
⁶⁰ Sun Yat-Sen University, Guangzhou 510275, People's Republic of China
⁶¹ Suranaree University of Technology, University Avenue 111, Nakhon Ratchasima 30000, Thailand
⁶² Tsinghua University, Beijing 100084, People's Republic of China
⁶³ Turkish Accelerator Center Particle Factory Group, (A)Istinye University, 34010, Istanbul, Turkey; (B)Near East University, Nicosia, North Cyprus, 99138, Mersin 10, Turkey
⁶⁴ University of Bristol, H H Wills Physics Laboratory, Tyndall Avenue, Bristol, BS8 1TL, UK
⁶⁵ University of Chinese Academy of Sciences, Beijing 100049, People's Republic of China
⁶⁶ University of Groningen, NL-9747 AA Groningen, The Netherlands
⁶⁷ University of Hawaii, Honolulu, Hawaii 96822, USA
⁶⁸ University of Jinan, Jinan 250022, People's Republic of China
⁶⁹ University of Manchester, Oxford Road, Manchester, M13 9PL, United Kingdom
⁷⁰ University of Muenster, Wilhelm-Klemm-Strasse 9, 48149 Muenster, Germany
⁷¹ University of Oxford, Keble Road, Oxford OX13RH, United Kingdom
⁷² University of Science and Technology Liaoning, Anshan 114051, People's Republic of China
⁷³ University of Science and Technology of China, Hefei 230026, People's Republic of China
⁷⁴ University of South China, Hengyang 421001, People's Republic of China
⁷⁵ University of the Punjab, Lahore-54590, Pakistan
⁷⁶ University of Turin and INFN, (A)University of Turin, I-10125, Turin, Italy; (B)University of Eastern Piedmont, I-15121, Alessandria, Italy; (C)INFN, I-10125, Turin, Italy
⁷⁷ Uppsala University, Box 516, SE-75120 Uppsala, Sweden
⁷⁸ Wuhan University, Wuhan 430072, People's Republic of China
⁷⁹ Yantai University, Yantai 264005, People's Republic of China
⁸⁰ Yunnan University, Kunming 650500, People's Republic of China
⁸¹ Zhejiang University, Hangzhou 310027, People's Republic of China
⁸² Zhengzhou University, Zhengzhou 450001, People's Republic of China
- ^a Deceased
^b Also at the Moscow Institute of Physics and Technology, Moscow 141700, Russia
^c Also at the Novosibirsk State University, Novosibirsk, 630090, Russia
^d Also at the NRC "Kurchatov Institute", PNPI, 188300, Gatchina, Russia
^e Also at Goethe University Frankfurt, 60323 Frankfurt am Main, Germany
^f Also at Key Laboratory for Particle Physics, Astrophysics and Cosmology, Ministry of Education; Shanghai Key Laboratory for Particle Physics and Cosmology; Institute of Nuclear and Particle Physics, Shanghai 200240, People's Republic of China
^g Also at Key Laboratory of Nuclear Physics and Ion-beam Application (MOE) and Institute of Modern Physics, Fudan University, Shanghai 200443, People's Republic of China
^h Also at State Key Laboratory of Nuclear Physics and Technology, Peking University, Beijing 100871, People's Republic of China
ⁱ Also at School of Physics and Electronics, Hunan University, Changsha 410082, China
^j Also at Guangdong Provincial Key Laboratory of Nuclear Science, Institute of Quantum Matter, South China Normal

University, Guangzhou 510006, China

^k Also at MOE Frontiers Science Center for Rare Isotopes, Lanzhou University, Lanzhou 730000, People's Republic of China

^l Also at Lanzhou Center for Theoretical Physics, Lanzhou University, Lanzhou 730000, People's Republic of China

^m Also at the Department of Mathematical Sciences, IBA, Karachi 75270, Pakistan

ⁿ Also at Ecole Polytechnique Federale de Lausanne (EPFL), CH-1015 Lausanne, Switzerland

^o Also at Helmholtz Institute Mainz, Staudinger Weg 18, D-55099 Mainz, Germany

^p Also at Hangzhou Institute for Advanced Study, University of Chinese Academy of Sciences, Hangzhou 310024, China

Using e^+e^- annihilation data corresponding to a total integrated luminosity of 7.33 fb^{-1} collected at center-of-mass energies between 4.128 and 4.226 GeV with the BESIII detector, we provide the first amplitude analysis and absolute branching fraction measurement of the hadronic decay $D_s^+ \rightarrow K_S^0 K_L^0 \pi^+$. The branching fraction of $D_s^+ \rightarrow K_S^0 K_L^0 \pi^+$ is determined to be $(1.86 \pm 0.06_{\text{stat}} \pm 0.03_{\text{syst}})\%$. Combining the $\mathcal{B}(D_s^+ \rightarrow \phi(\rightarrow K_S^0 K_L^0) \pi^+)$ obtained in this work and the world average of $\mathcal{B}(D_s^+ \rightarrow \phi(\rightarrow K^+ K^-) \pi^+)$, we measure the relative branching fraction $\mathcal{B}(\phi \rightarrow K_S^0 K_L^0)/\mathcal{B}(\phi \rightarrow K^+ K^-) = (0.597 \pm 0.023_{\text{stat}} \pm 0.018_{\text{syst}} \pm 0.016_{\text{PDG}})$, which deviates from the PDG value by more than 3σ . Furthermore, the asymmetry of the branching fractions of $D_s^+ \rightarrow K_S^0 K^*(892)^+$ and $D_s^+ \rightarrow K_L^0 K^*(892)^+$, $\frac{\mathcal{B}(D_s^+ \rightarrow K_S^0 K^*(892)^+) - \mathcal{B}(D_s^+ \rightarrow K_L^0 K^*(892)^+)}{\mathcal{B}(D_s^+ \rightarrow K_S^0 K^*(892)^+) + \mathcal{B}(D_s^+ \rightarrow K_L^0 K^*(892)^+)}$, is determined to be $(-13.4 \pm 5.0_{\text{stat}} \pm 3.4_{\text{syst}})\%$.

The ϕ meson, with a large proportion of $s\bar{s}$ and a mass in the non-perturbative Quantum Chromodynamics (QCD) region, is considered a potential carrier of the interaction between hadrons, as proposed in Hideki Yukawa's Meson Exchange theory [1]. It is also a valuable probe for studying QCD matter formed in relativistic heavy-ion collisions [2]. Consequently, the precise measurement of its decay characteristics holds significant theoretical and experimental value for investigating the non-perturbative behavior of the strong interaction and the properties of the nuclear force between baryons [3], thus deepening understanding of the structure of hadronic matter. In B physics, the accurate branching fractions (BFs) of ϕ decays are also essential input parameters for measurements of CP violation in golden decay modes, such as $B_{(s)} \rightarrow \phi\phi$ [4], $B \rightarrow \phi K$ [5], $B \rightarrow \phi\phi K$ [6], and $B \rightarrow J/\psi\phi K$ [7].

About 80% of ϕ mesons decay into $\phi \rightarrow K\bar{K}$, and the relative BF, $R_\phi \equiv \mathcal{B}(\phi \rightarrow K_S^0 K_L^0)/\mathcal{B}(\phi \rightarrow K^+ K^-)$, is naively expected to equal 0.5 due to isospin symmetry. Different theoretical predictions of R_ϕ , however, fall within a relatively large range of 0.62–0.71 [8–11], taking into account phase-space difference, radiative corrections, isospin breaking etc. The experimental measurements of R_ϕ currently range from 0.64 to 0.89 [12–16]. It is evident that although there is overlap between theoretical predictions and experimental measurements, further studies are required.

The Particle Data Group (PDG) average value of $R_\phi = 0.740 \pm 0.031$ [12] has not been updated for nearly 30 years¹ and the measurements were primarily made

40 to 50 years ago with e^+e^- annihilation and $K-p$ scattering experiments [12, 17–20], which usually suffer challenges from complex background and various interferences. Recently, Ref. [21] used total cross section measurements of the processes $e^+e^- \rightarrow K^+ K^- / K_S^0 K_L^0$, yielding a R_ϕ value of 0.644 ± 0.017 with the Unitary & Analytic model, suggesting the possibility that the experimental average may not be a reliable estimate of R_ϕ anymore. Therefore, exploring the reasons behind these differences and understanding the underlying mechanisms affecting ϕ meson decays requires a new and more accurate method to determine the BF of ϕ decays. The measurement of the BF of $D_s^+ \rightarrow \phi(\rightarrow K_S^0 K_L^0) \pi^+$, along with $D_s^+ \rightarrow \phi(\rightarrow K^+ K^-) \pi^+$ [22], serves as a new approach to determine R_ϕ in a more controlled environment. In addition, the BESIII Collaboration found that the measured BF ratio $\mathcal{B}(\phi \rightarrow \pi^+ \pi^- \pi^0)/\mathcal{B}(\phi \rightarrow K^+ K^-)$ deviates from the world average value by more than 4σ [23]. This further stimulates the urgent study of ϕ decay in the amplitude analysis of $D_s^+ \rightarrow K_S^0 K_L^0 \pi^+$ to explore the source of this tension.

Moreover, the symmetry $\Gamma(\bar{K}^0) = 2\Gamma(K_S^0) = 2\Gamma(K_L^0)$ is usually used for the decay modes containing a neutral kaon K_S^0 or K_L^0 . However, it is expected that the interference between Cabibbo-Favored (CF) and Doubly-Cabibbo-Suppressed (DCS) transitions could lead to a significant asymmetry, called $K_S^0 - K_L^0$ asymmetry [24–29]. The $K_S^0 - K_L^0$ asymmetry has not been observed in the $D \rightarrow K_{S,L}^0 + \text{Vector}$ system [30–32]. Phenomenological models, such as factorization-assisted topological-amplitude (FAT)[27] and topological diagram approach (DAT)[29], predict non-zero $K_S^0 - K_L^0$ asymmetry in the decay process of $D_s^+ \rightarrow K_{S,L}^0 + \text{Vector}$. Measurements for the $K_S^0 - K_L^0$ asymmetries serve as critical constraints on the dynamic models of charmed meson decays. In the amplitude analysis of $D_s^+ \rightarrow$

¹ While updated measurements of R_ϕ were reported by *CMD-2*, [?], and *CMD-3* [?] experiments in 1995 and 2018, respectively, they have not been taken into account for the averages by PDG.

$K_S^0 K_L^0 \pi^+$, the asymmetry of $D_s^+ \rightarrow K_S^0 K^*(892)^+$ and $D_s^+ \rightarrow K_L^0 K^*(892)^+$ can be measured with most systematic uncertainties cancelled. The obtained result will be crucial to better understand the dynamics of CF and DCS transitions.

In this Letter, we present the first amplitude analysis and absolute BF measurement of the $D_s^+ \rightarrow K_S^0 K_L^0 \pi^+$ decay using 7.33 fb^{-1} data samples collected at center-of-mass (CM) energies between $4.128\text{-}4.226 \text{ GeV}$ with the BESIII detector. Charge conjugation is implied throughout this Letter.

The BESIII detector [33, 34] records symmetric e^+e^- collisions provided by the BEPCII storage ring [35]. The cylindrical core of the BESIII detector covers 93% of the full solid angle and consists of a helium-based multilayer drift chamber, a plastic scintillator time-of-flight system (TOF), and a CsI(Tl) electromagnetic calorimeter (EMC), which are all enclosed in a superconducting solenoidal magnet providing a 1.0 T magnetic field. The end cap TOF system was upgraded in 2015 using multi-gap resistive plate chamber technology, providing a time resolution of 60 ps, which benefits 83% of the data used in this analysis [36].

Simulated data samples produced with GEANT4-based [37] Monte Carlo (MC) software, which includes the geometric description of the BESIII detector and the detector response, are used to determine detection efficiencies and to estimate backgrounds. The simulation models the beam energy spread and initial state radiation (ISR) in the e^+e^- annihilations with the generator KKMC [38]. The inclusive MC sample includes the production of open charm processes, the ISR production of vector charmonium(-like) states, and the continuum processes. All particle decays are modeled with EVTGEN [39] using BFs either taken from the PDG [12], when available, or otherwise estimated with LUNDCHARM [40]. Final-state radiation from charged final-state particles is incorporated using the PHOTOS package [41].

The process $e^+e^- \rightarrow D_s^{*\pm} D_s^\mp \rightarrow \gamma D_s^+ D_s^-$ allows studies of D_s^+ decays using a tag technique [42, 43]. Two types of samples are used: single tag (ST) and double tag (DT). In the ST sample, a D_s^- , designated as “tag”, is reconstructed through one of ten hadronic decay modes: $K_S^0 K^-$, $K^+ K^- \pi^-$, $K_S^0 K^- \pi^0$, $K^+ K^- \pi^- \pi^0$, $K_S^0 K^- \pi^- \pi^+$, $K_S^0 K^+ \pi^- \pi^-$, $\pi^- \pi^- \pi^+$, $\pi^- \eta$, $\pi^- \eta'$, and $K^- \pi^- \pi^+$. In the DT sample, a D_s^+ , designated as the “signal”, is reconstructed through $D_s^+ \rightarrow K_S^0 K_L^0 \pi^+$. A detailed description of selection conditions concerning charged and neutral particle candidates, the mass recoiling against D_s^\pm candidates, and the mass of the tag candidates are provided in Refs. [44–48].

After a D_s^- tag candidate is identified, we reconstruct the signal $D_s^+ \rightarrow K_S^0 K_L^0 \pi^+$ candidate recoiling against the tag by requiring two positively charged particles iden-

tified as π^+ , one negatively π^- , and at least one more photon to reconstruct the transition photon of $D_s^{*\pm} \rightarrow \gamma D_s^\pm$. The four-momentum of the K_L^0 needs to be determined, which is calculated with the momentum of the initial e^+e^- system and other detected particles. If there are multiple signal candidates for K_S^0 , the best candidate with the minimum χ^2 of a four-constraint (4C) kinematic fit is chosen. The total four-momentum is constrained to the four-momentum of the initial e^+e^- beams. The invariant masses of the tag D_s^- , the signal D_s^+ , the D_s^* , and K_S^0 are constrained to their PDG values [12]. The two cases $D_s^{*\pm} \rightarrow D_s^+ \gamma$ and $D_s^{*\pm} \rightarrow D_s^- \gamma$ are considered. The combination with the minimum χ^2 is chosen. Furthermore, the square of the recoil mass against the transition photon and the tag $D_s^- (M_{\text{rec}}'^2)$ is expected to peak at the known D_s^\pm meson mass squared before the kinematic fit for signal $D_s^{*\pm} D_s^\mp$ events, and must satisfy $3.80 < M_{\text{rec}}'^2 < 4.0 \text{ GeV}^2/c^4$. The requirement that the number of additional $\pi^0 (N_{\pi^0})$ composed of unused photons in the ST candidate selection and $D_s^{*\pm} \rightarrow \gamma D_s^\pm$ is equal to zero is applied to suppress backgrounds. Here, since K_L^0 may cause fake photons in the EMC, the angles of any photons that form π^0 s and the shower produced by K_L^0 are required to be greater than 10° .

The purity is determined by fitting the missing mass squared (M_{miss}^2) of the K_L^0 candidates after the 4C kinematic fit, which is defined as

$$M_{\text{miss}}^2 = \frac{1}{c^2} (\vec{p}_{\text{CM}} - \vec{p}_{\text{tag}} - \vec{p}_{K_S^0} - \vec{p}_{\pi^+} - \vec{p}_\gamma)^2, \quad (1)$$

where \vec{p}_{CM} is the momentum of the e^+e^- CM system, \vec{p}_{tag} and \vec{p}_i ($i = K_S^0, \pi^+, \gamma$) are the four-momenta of the tag candidate and the final-state particle i on the signal side. The M_{miss}^2 mass window, $[0.21, 0.29] \text{ GeV}^2/c^4$, is applied on the signal candidates for the amplitude analysis. In total, 2310 events are selected with a purity of $f_s = (78.2 \pm 1.0)\%$. Here, the peaking background from $D_s^+ \rightarrow K_S^0 K_L^0 \pi^+$ is 4.3%, and simulated based on the amplitude analysis by BESIII [48].

Based on the 4C kinematic fit, an additional constraint on the mass of K_L^0 is added (5C) and the four-momenta of the final-state particles of the 5C kinematic fit are used for the amplitude analysis to ensure that all candidates fall within the phase-space boundary. The isobar formulation is used in the covariant tensor formalism [49]. The total signal amplitude $\mathcal{M} = \sum \rho_n e^{i\varphi_n} A_n$, is described by a coherent sum of the amplitudes from all intermediate processes, where n represents the n^{th} intermediate state with magnitude ρ_n and phase φ_n . The decay amplitude A_n is given by $A_n = P_n S_n F_n^r F_n^D$, where S_n and $F_n^r(D)$ are the spin factor [49] and the Blatt-Weisskopf barrier factor of the intermediate state (the D_s^\pm meson) [50], respectively, and P_n is the propagator of the intermediate resonance, which is the relativistic Breit-Wigner amplitude [51].

The unbinned maximum likelihood method is adopted in the amplitude analysis. A combined probability density function (PDF) for the signal and background hypotheses is constructed, with the four-momenta of the final-state particles. The signal PDF is constructed from the total amplitude \mathcal{M} . The background PDF, B , is constructed from a background shape derived from the inclusive MC samples using the XGBoost package [52, 53]. This background PDF is then added to the signal PDF incoherently. The likelihood function is written as

$$\mathcal{L} = \prod_j \left[\frac{\epsilon f_s |\mathcal{M}(p_j^\mu)|^2 R_3}{\int \epsilon |\mathcal{M}(p_j^\mu)|^2 R_3 dp_j} + \frac{(1-f_s)B(p_j^\mu)R_3}{\int B(p_j^\mu) R_3 dp_j} \right], \quad (2)$$

where j runs over the selected events, p_j^μ represents the four-momenta of the final-state particles, and ϵ is the detection efficiency determined with a MC sample of $D_s^+ \rightarrow K_S^0 K_L^0 \pi^+$ uniformly distributed over the Dalitz plot. Ultimately, f_s and R_3 denote the purity and three-body phase-space element, respectively. The normalization integral in the denominator is determined by an MC technique as described in Refs. [45–48, 54].

The Dalitz plot of $M_{K_L^0 \pi^+}^2$ versus $M_{K_S^0 \pi^+}^2$ from all data samples is shown in Fig. 1(a). The slant band in the upper right corner is caused by the process $D_s^+ \rightarrow \phi \pi^+$, the vertical and horizontal bands around 0.8 GeV^2/c^4 are $D_s^+ \rightarrow K_L^0 K^*(892)^+$ and $D_s^+ \rightarrow K_S^0 K^*(892)^+$, respectively. The $D_s^+ \rightarrow \phi \pi^+$ process is used as a reference so

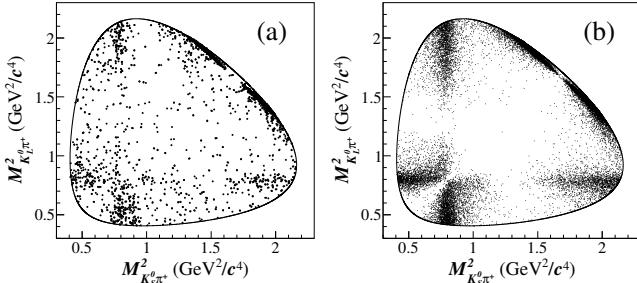


FIG. 1. Dalitz plots of $M_{K_L^0 \pi^+}^2$ versus $M_{K_S^0 \pi^+}^2$ for $D_s^+ \rightarrow K_S^0 K_L^0 \pi^+$, of (a) the sum of all data samples and (b) the signal MC samples generated based on the amplitude analysis. The black curve indicates the kinematic boundary.

that the magnitudes and phases of other amplitudes can be fitted as relative values to this reference amplitude. The purity is fixed in the fit. Other possible contributing resonances such as $K_1(1410)^+$, $K_0^*(1430)^+$, $K_2^*(1430)^+$, $(K_S^0 \pi^+)_{S\text{-wave}}$, $(K_L^0 \pi^+)_{S\text{-wave}}$, and $\phi(1680)$ are added to the fit one at a time. The masses and widths of all resonances are fixed to their PDG values [12]. The statistical significance of each new amplitude is calculated from the change of the log-likelihood taking the change in the number of degrees of freedom into account. Various combinations of these resonances are also tested. Only the amplitudes $D_s^+ \rightarrow \phi \pi^+$, $D_s^+ \rightarrow K_L^0 K^*(892)^+$, and

$D_s^+ \rightarrow K_S^0 K^*(892)^+$ are found, and no other contribution has a significance greater than 5σ . The Dalitz plot of the signal MC sample generated based on the result of the amplitude analysis is shown in Fig. 1(b). The mass projections of the fit are shown in Fig. 2.

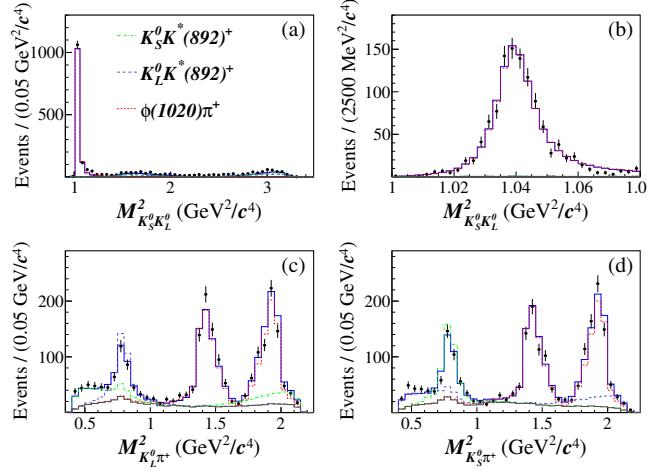


FIG. 2. Distributions of (a) $M_{K_S^0 K_L^0}^2$, (b) $M_{K_S^0 K_L^0}^2$ around the ϕ peak, (c) $M_{K_L^0 \pi^+}^2$ and (d) $M_{K_S^0 \pi^+}^2$ from the nominal fit. The data samples are represented by points with error bars, the fit results by blue lines, and the backgrounds by gray lines. Colored dashed lines show the individual components of the fit model.

The contribution of the n^{th} amplitude relative to the total BF is quantified by the fit fraction (FF) defined as $\text{FF}_n = \int |\rho_n A_n|^2 R_3 dp_j / \int |\mathcal{M}|^2 R_3 dp_j$. The FFs of both amplitudes and the phase differences relative to the reference process are listed in Table I. The sum of the three FFs is 111.0%. The asymmetry of the branching fractions of $D_s^+ \rightarrow K_S^0 K^*(892)^+$ and $D_s^+ \rightarrow K_L^0 K^*(892)^+$ is determined to be $\frac{\mathcal{B}(D_s^+ \rightarrow K_S^0 K^*(892)^+) - \mathcal{B}(D_s^+ \rightarrow K_L^0 K^*(892)^+)}{\mathcal{B}(D_s^+ \rightarrow K_S^0 K^*(892)^+) + \mathcal{B}(D_s^+ \rightarrow K_L^0 K^*(892)^+)} = (-13.4 \pm 5.0_{\text{stat}} \pm 3.4_{\text{syst}})\%$, where the correlation of uncertainties between $D_s^+ \rightarrow K_S^0 K^*(892)^+$ and $D_s^+ \rightarrow K_L^0 K^*(892)^+$ is considered.

The systematic uncertainties related to the amplitude analysis, including the phase difference, FFs and $K_S^0 - K_L^0$ asymmetry, are determined by the differences between the results of the nominal fit and the alternative fits. The masses and widths of the ϕ and $K^*(892)^+$ are shifted by their uncertainties [12]. The radii of the Blatt-Weisskopf barrier factors are varied from their nominal values of 5 GeV^{-1} and 3 GeV^{-1} (for the D_s^+ meson and the intermediate resonances, respectively) by $\pm 1 \text{ GeV}^{-1}$. The uncertainties associated with the size of the background sample are studied by varying the purity within its statistical uncertainty. An alternative background sample is used to determine the background PDF, where the relative fractions of background processes from direct $q\bar{q}$ and non- $D_s^{*\pm} D_s^{\mp}$ open-charm processes are varied by the sta-

TABLE I. Phases, FFs, BFs, and statistical significances (σ) of intermediate processes in $D_s^+ \rightarrow K_S^0 K_L^0 \pi^+$. The first and second uncertainties are statistical and systematic, respectively.

Amplitude	Phase (rad)	FF (%)	BF (%)	σ
$D_s^+ \rightarrow \phi\pi^+$	0.0(fixed)	$70.9 \pm 1.3 \pm 1.5$	$1.32 \pm 0.05 \pm 0.04 > 10$	
$D_s^+ \rightarrow K_L^0 K^*(892)^+$	$0.68 \pm 0.17 \pm 0.21$	$22.8 \pm 1.3 \pm 1.5$	$0.42 \pm 0.03 \pm 0.03 > 10$	
$D_s^+ \rightarrow K_S^0 K^*(892)^+$	$-2.40 \pm 0.18 \pm 0.31$	$17.4 \pm 1.2 \pm 0.9$	$0.31 \pm 0.02 \pm 0.02 > 10$	

tistical uncertainties of the known cross sections. The uncertainty from the peaking background is also considered based on the uncertainty from the measurement of $D_s^+ \rightarrow K_S^0 K_S^0 \pi^+$ [12] with one $K_S^0 \rightarrow \pi^0 \pi^0$. In addition, we perform the input/output checks, taking the deviations as the corresponding systematic uncertainties. The intermediate resonances with statistical significances less than 5σ , such as $K_1(1410)^+$, $K_0^*(1430)^+$, $K_2^*(1430)^+$, $(K_S^0 \pi^+)_S$ -wave, $(K_L^0 \pi^+)_S$ -wave, and $\phi(1680)$, are taken as the systematic uncertainty. The total uncertainties are obtained by adding these contributions in quadrature. Details can be found in Supplemental Material [55]. In addition, the correlated systematic uncertainties of the asymmetry of the branching fractions of $D_s^+ \rightarrow K_S^0 K^*(892)^+$ and $D_s^+ \rightarrow K_L^0 K^*(892)^+$ can be considered and reduced.

The BF measurement method of $D_s^+ \rightarrow K_S^0 K_L^0 \pi^+$ is essentially the same as the amplitude analysis, with the only difference being that we no longer impose requirements on $N_{\pi^0} = 0$ and $0.21 < M_{\text{miss}}^2 < 0.29 \text{ GeV}^2/c^4$, as we aim to avoid the systematic uncertainties they may introduce. The BF is given by [45, 46]

$$\mathcal{B}_{\text{sig}} = \frac{N_{\text{total,sig}}^{\text{DT}}}{\mathcal{B}_{\text{sub}} \sum_{\alpha,i} N_{\alpha,i}^{\text{ST}} \epsilon_{\alpha,\text{sig},i}^{\text{DT}} / \epsilon_{\alpha,i}^{\text{ST}}}, \quad (3)$$

where α runs over the various tag modes, and i denotes the different CM energies, and \mathcal{B}_{sub} represent the BFs of all possible intermediate particles. The ST yields in data $N_{\alpha,i}^{\text{ST}}$ and the DT yield $N_{\text{total,sig}}^{\text{DT}}$ are determined by fitting the mass of D_s^- and M_{miss}^2 distributions, respectively. The fit to the M_{miss}^2 distribution is shown in Fig. 3. The signal shape is modeled with the MC-simulated shape convolved with a Gaussian function. The dominant peaking background is $D_s^+ \rightarrow K_S^0 K_S^0 \pi^+$ with one $K_S^0 \rightarrow \pi^0 \pi^0$. This peaking background is modeled by the MC-simulated shape based on the amplitude analysis [48], with a size Gaussian-constrained to the expected yield 584 ± 33 according to its measured BF [12]. The shape of other backgrounds is derived from the inclusive MC samples and its size is floated in the fit. The corresponding efficiencies ϵ are obtained by analyzing the inclusive MC samples, with the signal MC events of $D_s^+ \rightarrow K_S^0 K_L^0 \pi^+$ generated based on the results of the amplitude analysis. The details of ST yields, ST efficiencies, and DT efficiencies can be found in the

Supplemental Material [55]. The total ST yields of all tag modes and the DT yields are 665265 ± 2750 and 2349 ± 76 , respectively. The BF of $D_s^+ \rightarrow K_S^0 K_L^0 \pi^+$ is determined to be $(1.86 \pm 0.06_{\text{stat}} \pm 0.03_{\text{syst}})\%$.

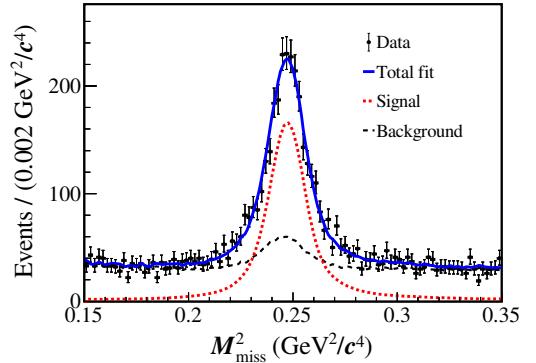


FIG. 3. Fit to the M_{miss}^2 distribution of the DT signal candidates. The data samples are represented by points with error bars, the signal contributions by the red dashed line, the total fit results by the solid blue line, and the background contributions by the dashed black line.

The following systematic uncertainties are considered in the BF measurement. The uncertainty in the total number of ST D_s^- mesons is assigned to be 0.4%. The uncertainty related to a non-peaking background shape in the fit to a M_{miss}^2 distribution is assigned by repeating the fit with the MC background components varied by $\pm 30\%$. The π^+ particle identification and tracking efficiencies are studied with $e^+e^- \rightarrow K^+ K^- \pi^+ \pi^-$ and the corresponding uncertainties are assigned to be 0.5% and 0.2%, respectively. The uncertainty for the K_S^0 reconstruction is 1.0% using control samples of $J/\psi \rightarrow K_S^0 K^\pm \pi^\mp$ and $J/\psi \rightarrow \phi K_S^0 K^\pm \pi^\mp$. The systematic uncertainty of photon reconstruction is assigned as 1.0% with the control sample of $D_s^+ \rightarrow K_S^0 K^+$. The uncertainty from the signal MC model based on the results of the amplitude analysis is studied by varying the fit parameters according to the covariance matrix. The change of signal efficiency, 0.1%, is assigned as the uncertainty. The uncertainties from the quoted BFs of $K_S^0 \rightarrow \pi^+ \pi^-$ and $D_s^{*\pm} \rightarrow \gamma D_s^\pm$ are 0.1% and 0.4% [12], respectively. The uncertainty due to the limited signal MC sample size is 0.3%. The total

uncertainty is determined by adding all the contributions in quadrature and is 1.6%.

In summary, we have presented the first amplitude analysis and BF measurement of the hadronic decay $D_s^+ \rightarrow K_S^0 K_L^0 \pi^+$ using 7.33 fb^{-1} of e^+e^- annihilation data taken at CM energies between 4.128 and 4.226 GeV. The amplitude analysis results are listed in Table I. With a detection efficiency obtained based on the amplitude analysis model, we obtain $\mathcal{B}(D_s^+ \rightarrow K_S^0 K_L^0 \pi^+) = (1.86 \pm 0.06_{\text{stat}} \pm 0.03_{\text{syst}})\%$. The BFs of intermediate processes are calculated via $\mathcal{B}_i = \text{FF}_i \times \mathcal{B}(D_s^+ \rightarrow K_S^0 K_L^0 \pi^+)$ and $\mathcal{B}(D_s^+ \rightarrow \phi \pi^+, \phi \rightarrow K_S^0 K_L^0)$ is determined to be $(1.32 \pm 0.05_{\text{stat}} \pm 0.04_{\text{syst}})\%$. With the PDG value of $\mathcal{B}(D_s^+ \rightarrow \phi \pi^+, \phi \rightarrow K^+ K^-) = (2.21 \pm 0.06)\%$ [12], we determine a relative BF between $\phi \rightarrow K_S^0 K_L^0$ and $\phi \rightarrow K^+ K^-$ to be $R_\phi = (0.597 \pm 0.023_{\text{stat}} \pm 0.018_{\text{syst}} \pm 0.016_{\text{PDG}})$, where the third error is due to the uncertainty of the PDG value of $\mathcal{B}(D_s^+ \rightarrow \phi \pi^+, \phi \rightarrow K^+ K^-)$ [12]. The obtained R_ϕ is consistent with theoretical expectations as reported in Ref.[8]. However, it is $(1.0 - 2.8)\sigma$ below all previous measurements, see Fig. 4, and deviates from the PDG average (PDG fit) by 3.2σ (2.6σ). Note that the earlier measurement of $\mathcal{B}(\phi \rightarrow \pi^+ \pi^- \pi^0)/\mathcal{B}(\phi \rightarrow K^+ K^-)$ by BESIII[23] also significantly deviates from the PDG values that were obtained in e^+e^- annihilation and $K - p$ scattering experiments. To further explore the reasons behind these differences and to understand the underlying mechanisms that influence the BFs of ϕ meson decays, more precise measurements are needed in the future.

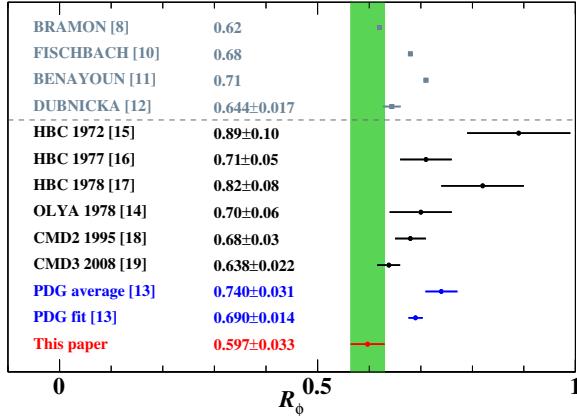


FIG. 4. Comparison of the results for R_ϕ measured in this analysis and the HBC, OLYA, CMD2, and CMD3 experiments. Above the dotted line are the theoretical calculations, below are the experimental results. The green band present the total uncertainty obtained in this work.

In addition, the $K_S^0 - K_L^0$ asymmetry in $D_s^+ \rightarrow \bar{K}^0 K^{*+}$ is determined to be $\frac{\mathcal{B}(D_s^+ \rightarrow K_S^0 K^{*(892)^+}) - \mathcal{B}(D_s^+ \rightarrow K_L^0 K^{*(892)^+})}{\mathcal{B}(D_s^+ \rightarrow K_S^0 K^{*(892)^+}) + \mathcal{B}(D_s^+ \rightarrow K_L^0 K^{*(892)^+})} = (-13.4 \pm$

$5.0_{\text{stat}} \pm 3.4_{\text{syst}})\%$. The predicted $K_S^0 - K_L^0$ asymmetries from different approaches, as well as the measured value, are summarized in Table II. This is the first observation of the $K_S^0 - K_L^0$ asymmetry in the $D \rightarrow K_{S,L}^0 + \text{Vector}$ system of charmed meson decays.

The BESIII Collaboration thanks the staff of BEPCII and the IHEP computing center for their strong support. This work is supported in part by National Key R&D Program of China under Contracts Nos. 2023YFA1606000, 2023YFA1606704; National Natural Science Foundation of China (NSFC) under Contracts Nos. 123B2077, 12035009, 11635010, 11735014, 11935015, 11935016, 11935018, 12025502, 12035013, 12061131003, 12192260, 12192261, 12192262, 12192263, 12192264, 12192265, 12221005, 12225509, 12235017, 12361141819; the Chinese Academy of Sciences (CAS) Large-Scale Scientific Facility Program; the CAS Center for Excellence in Particle Physics (CCEPP); Joint Large-Scale Scientific Facility Funds of the NSFC and CAS under Contract No. U1832207, U2032104; CAS under Contract No. YSBR-101; 100 Talents Program of CAS; The Excellent Youth Foundation of Henan Scientific Committee under Contract No. 242300421044; The Institute of Nuclear and Particle Physics (INPAC) and Shanghai Key Laboratory for Particle Physics and Cosmology; Agencia Nacional de Investigación y Desarrollo de Chile (ANID), Chile under Contract No. ANID PIA/APOYO AFB230003; German Research Foundation DFG under Contract No. FOR5327; Istituto Nazionale di Fisica Nucleare, Italy; Knut and Alice Wallenberg Foundation under Contracts Nos. 2021.0174, 2021.0299; Ministry of Development of Turkey under Contract No. DPT2006K-120470; National Research Foundation of Korea under Contract No. NRF-2022R1A2C1092335; National Science and Technology fund of Mongolia; National Science Research and Innovation Fund (NSRF) via the Program Management Unit for Human Resources & Institutional Development, Research and Innovation of Thailand under Contract No. B50G670107; Polish National Science Centre under Contract No. 2019/35/O/ST2/02907; Swedish Research Council under Contract No. 2019.04595; The Swedish Foundation for International Cooperation in Research and Higher Education under Contract No. CH2018-7756; U. S. Department of Energy under Contract No. DE-FG02-05ER41374.

-
- [1] Hideki Yukawa, *Proc. Phys. Math. Soc. Jap.* **17**, (1935) 48-57, *Prog. Theor. Phys. Suppl.* **1** 1-10.
 - [2] M. S. Abdallah *et al.* (STAR Collaboration), *Nature* **614**, 224-248, (2023).
 - [3] M. M. Nagels and Th. A. Rijken, *Phys. Rev. C* **99**, 044002 (2019).

TABLE II. Predictions for $K_S^0 - K_L^0$ asymmetries in $D_s^+ \rightarrow \bar{K}^0 K^{*+}$ decays from different phenomenological models and our measurement result.

Model	DAT(F4)	DAT(F1')	FAT	This work
$D_s^+ \rightarrow \bar{K}^0 K^{*+}$	-0.164 ± 0.032	-0.159 ± 0.028	-0.070 ± 0.032	$-0.134 \pm 0.050 \pm 0.034$

- [4] Ia. Bezshyiko *et al.* (LHCb Collaboration), *Phys. Rev. Lett.* **131**, 171802 (2023).
- [5] D. Acosta *et al.* (CDF Collaboration), *Phys. Rev. Lett.* **95**, 031801 (2005).
- [6] B. Aubert *et al.* (BaBar Collaboration), *Phys. Rev. Lett.* **97**, 261803 (2006).
- [7] B. Aubert *et al.* (BaBar Collaboration), *Phys. Rev. Lett.* **91**, 071801 (2003).
- [8] A. Bramon, R. Escrivano, J. L. LucioM, and G. Pancheri, *Phys. Lett. B* **486**, 406 (2000).
- [9] F. V. Flores-Baez, G. Lopez Castro, *Phys. Rev. D* **78**, 077301 (2008).
- [10] E. Fischbach, A. W. Overhauser, B. Woodahl, *Phys. Lett. B* **526**, 355 (2002).
- [11] M. Benayoun, P. David, L. DelBuono, F. Jegerlehner, *Eur. Phys. J. C* **72**, 1848 (2012).
- [12] S. Navas *et al.* (Particle Data Group), *Phys. Rev. D* **110**, 030001 (2024).
- [13] A. D. Bukanin, L. M. Kurdadze, S. I. Serednyakov, V. A. Sidorov, A. N. Skrinsky, Yu. M. Shatunov, B. A. Shvarts, and S. I. Eidelman, *Sov. J. Nucl. Phys.* **27**, 516 (1978).
- [14] M. A. Benitez, S. U. Chung, R. L. Eisner, and N. P. Samios, *Phys. Rev. D* **6**, 29 (1972).
- [15] H. Laven, *et al.* (Aachen-Berlin-CERN-London-Vienna Collaboration), *Nucl. Phys. B* **127**, 43 (1977).
- [16] M. J. Losty, *et al.* (Amsterdam-CERN-Nijmegen-Oxford Collaboration), *Nucl. Phys. B* **133**, 38 (1978).
- [17] G. Parrou, G. Cosme, A. Courau, B. Dudelzak *et al.*, *Phys. Lett. B* **63**, 357-361 (1976).
- [18] A. D. Bukanin, L. M. Kurdadze, S. I. Serednyakov, V. A. Sidorov *et al.*, *Yad. Fiz.* **27**, 976-984 (1978).
- [19] M. Mattiuzzi, A. Bracco, F. Camera, B. Million *et al.*, *Phys. Lett. B* **364**, 13-18 (1995).
- [20] S. I. Dolinsky, V. P. Druzhinin, M. S. Dubrovin, V. B. Golubev *et al.*, *Phys. Rept.* **202**, 99-170 (1991).
- [21] S. Dubnička, A. Z. Dubničková, L. Holka, and A. Liptaj, *Phys. Rev. D* **110** 054019 (2024).
- [22] M. Ablikim *et al.* (BESIII Collaboration), *Phys. Rev. D* **104**, 012016 (2021).
- [23] M. Ablikim *et al.* (BESIII Collaboration), *Phys. Rev. Lett.* **134**, 011904 (2025).
- [24] I. I. Bigi and H. Yamamoto, *Phys. Lett. B* **349**, 363 (1995).
- [25] J. L. Rosner, *Phys. Rev. D* **74**, 057502 (2006).
- [26] B. Bhattacharya and J. L. Rosner, *Phys. Rev. D* **81**, 014026 (2010).
- [27] D. Wang, F. S. Yu, P. F. Guo, and H. Y. Jiang, *Phys. Rev. D* **95**, 073007 (2017).
- [28] Sarah Müller, Ulrich Nierste, and Stefan Schacht, *Phys. Rev. D* **92**, 014004 (2015).
- [29] H. Y. Cheng and C. W. Chiang, *Phys. Rev. D* **109**, 073008 (2024).
- [30] Harry J. Lipkin, Z. Z. Xing, *Phys. Lett. B* **450**, 405 (1999).
- [31] D. N. Gao, *Phys. Lett. B* **645**, 59 (2007).
- [32] M. Ablikim *et al.* (BESIII Collaboration), *Phys. Rev. D* **105**, 092010 (2022).
- [33] M. Ablikim *et al.* (BESIII Collaboration), *Nucl. Instrum. Methods Phys. Res. Sect. A* **614**, 345 (2010).
- [34] M. Ablikim *et al.* (BESIII Collaboration), *Chin. Phys. C* **44**, 040001 (2020).
- [35] C. H. Yu *et al.*, Proceedings of IPAC2016, Busan, Korea, 2016, doi:10.18429/JACoW-IPAC2016-TUYA01.
- [36] X. Li *et al.*, *Radiat. Detect. Technol. Methods* **1**, 13 (2017); Y. X. Guo *et al.*, *Radiat. Detect. Technol. Methods* **1**, 15 (2017). P. Cao *et al.*, *Nucl. Instrum. Meth. A* **953**, 163053 (2022).
- [37] S. Agostinelli *et al.* (GEANT4 Collaboration), *Nucl. Instrum. Meth. A* **506**, 250 (2003).
- [38] S. Jadach, B. F. L. Ward, and Z. Was, *Phys. Rev. D* **63**, 113009 (2001); *Comput. Phys. Commun.* **130**, 260 (2000).
- [39] D. J. Lange, *Nucl. Instrum. Meth. A* **462**, 152 (2001); R. G. Ping, *Chin. Phys. C* **32**, 599 (2008).
- [40] J. C. Chen, G. S. Huang, X. R. Qi, D. H. Zhang, and Y. S. Zhu, *Phys. Rev. D* **62**, 034003 (2000); R. L. Yang, R. G. Ping and H. Chen, *Chin. Phys. Lett.* **31**, 061301 (2014).
- [41] E. Barberio, B. van Eijk and Z. Was, *Comput. Phys. Commun.* **66**, 115 (1991).
- [42] J. Adler *et al.* (MARK-III Collaboration), *Phys. Rev. Lett.* **62**, 1821 (1989).
- [43] B. C. Ke, J. Koponen, H. B. Li and Y. Zheng, *Ann. Rev. Nucl. Part. Sci.* **73** (2023), 285-314.
- [44] M. Ablikim *et al.* (BESIII Collaboration), *Phys. Rev. D* **103**, 092004 (2021).
- [45] M. Ablikim *et al.* (BESIII Collaboration), *J. High Energ. Phys.* **06**, 181 (2021).
- [46] M. Ablikim *et al.* (BESIII Collaboration), *Phys. Rev. D* **103**, 092006 (2021).
- [47] M. Ablikim *et al.* (BESIII Collaboration), *Phys. Rev. Lett.* **129**, 182001 (2022).
- [48] M. Ablikim *et al.* (BESIII Collaboration), *Phys. Rev. D* **105**, L051103 (2022).
- [49] B. S. Zou and D. V. Bugg, *Eur. Phys. J. A* **16**, 537 (2003).
- [50] J. M. Blatt and V. F. Weisskopf, *Theoretical Nuclear Physics* (John Wiley & Sons, New York, 1973).
- [51] J. D. Jackson, *N. Cimento* **34**, 1644 (1964).
- [52] A. Rogozhnikov, *J. Phys. Conf. Ser.* **762** 012036(2016).
- [53] B. Liu, X. Xiong, G. Hou, S. Song, and L. Shen, *EPJ Web Conf.* **214**, 06033 (2019).
- [54] M. Ablikim *et al.* (BESIII Collaboration), *Phys. Rev. Lett.* **132**, 131903 (2024).
- [55] See Supplemental Material at Link for additional analysis information.

**SUPPLEMENTAL MATERIAL: STUDY OF
 $\phi \rightarrow K\bar{K}$ AND $K_S^0 - K_L^0$ ASYMMETRY IN THE
AMPLITUDE ANALYSIS OF $D_s^+ \rightarrow K_S^0 K_L^0 \pi^+$
DECAY**

Table III shows detailed values of systematic uncertainties due to (I) fixed parameters, (II) barrier radius, (III) background, (IV) fit bias, and (V) non-significant resonance in the amplitude analysis of $D_s^+ \rightarrow K_S^0 K_L^0 \pi^+$. The total uncertainties are determined by adding all the contributions in quadrature.

TABLE III. Systematic uncertainties on the ϕ , FFs, and $K_S^0 - K_L^0$ asymmetry for different amplitudes in units of the corresponding statistical uncertainties.

Source	I	II	III	IV	V	Total
$D_s^+ \rightarrow \phi\pi^+$	FF	0.04	0.64	0.94	0.07	0.22
$D_s^+ \rightarrow K_L^0 K^*(892)^+$	Phase	0.05	0.37	0.54	0.02	1.04
	FF	0.07	0.26	0.58	0.16	0.96
$D_s^+ \rightarrow K_S^0 K^*(892)^+$	Phase	0.03	0.34	0.54	0.02	1.57
	FF	0.11	0.38	0.52	0.01	0.31
$K_S^0 - K_L^0$ asymmetry		0.01	0.09	0.12	0.10	0.66
						0.68

Tables IV and V summarize the ST yields in data and the ST efficiencies at $\sqrt{s} = 4.128 - 4.226$ GeV, respectively.

TABLE IV. The ST yields yields in data (N^{ST}) at $\sqrt{s} =$ (I) 4.128 – 4.157, (II) 4.178, (III) 4.189 – 4.219, and (IV) 4.226 GeV, where uncertainties are statistical.

Tag mode	(I) N^{ST}	(II) N^{ST}	(III) N^{ST}	(IV) N^{ST}
$D_s^- \rightarrow K_S^0 K^-$	6728 \pm 144	31949 \pm 314	19960 \pm 270	6837 \pm 163
$D_s^- \rightarrow K_S^0 K^- \pi^-$	27670 \pm 280	137138 \pm 614	29644 \pm 335	29644 \pm 335
$D_s^- \rightarrow K_S^0 K^+ \pi^0$	1996 \pm 178	11310 \pm 529	2245 \pm 217	2245 \pm 217
$D_s^- \rightarrow K^+ K^- \pi^- \pi^0$	7457 \pm 397	39339 \pm 798	24693 \pm 688	8084 \pm 481
$D_s^- \rightarrow K_S^0 K^- \pi^- \pi^+$	1885 \pm 151	8086 \pm 328	5719 \pm 299	1659 \pm 214
$D_s^- \rightarrow K_S^0 K^+ \pi^- \pi^-$	2983 \pm 129	15704 \pm 288	9782 \pm 246	3379 \pm 173
$D_s^- \rightarrow \pi^- \pi^- \pi^+$	7312 \pm 374	37988 \pm 857	23210 \pm 804	7939 \pm 422
$D_s^- \rightarrow \pi^- \eta$	4355 \pm 373	18305 \pm 601	11130 \pm 891	3835 \pm 205
$D_s^- \rightarrow \pi^- \eta'_{\pi^+ \pi^- \eta \gamma \gamma}$	1515 \pm 64	7739 \pm 141	4774 \pm 115	1695 \pm 75
$D_s^- \rightarrow K^- \pi^+ \pi^-$	3804 \pm 345	17438 \pm 565	10840 \pm 469	5143 \pm 447

Table VI summarizes the DT efficiencies of $D_s^+ \rightarrow K_S^0 K_L^0 \pi^+$ at $\sqrt{s} = 4.128 - 4.226$ GeV.

TABLE V. The ST efficiencies (ϵ^{ST}) at $\sqrt{s} =$ (I) 4.128–4.157, (II) 4.178, (III) 4.189–4.219, and (IV) 4.226 GeV, where uncertainties are statistical.

Tag mode	(I) $\epsilon^{\text{ST}}(\%)$	(II) $\epsilon^{\text{ST}}(\%)$	(III) $\epsilon^{\text{ST}}(\%)$	(IV) $\epsilon^{\text{ST}}(\%)$
$D_s^- \rightarrow K_S^0 K^-$	47.64 \pm 0.06	47.39 \pm 0.07	47.23 \pm 0.09	47.95 \pm 0.16
$D_s^- \rightarrow K^+ K^- \pi^-$	40.37 \pm 0.07	39.47 \pm 0.03	39.33 \pm 0.04	39.78 \pm 0.07
$D_s^- \rightarrow K_S^0 K^+ \pi^0$	16.27 \pm 0.26	16.00 \pm 0.11	15.87 \pm 0.15	16.09 \pm 0.29
$D_s^- \rightarrow K^+ K^- \pi^- \pi^0$	10.59 \pm 0.08	10.68 \pm 0.03	10.74 \pm 0.05	10.89 \pm 0.09
$D_s^- \rightarrow K_S^0 K^- \pi^- \pi^+$	20.03 \pm 0.28	20.31 \pm 0.12	20.24 \pm 0.16	20.28 \pm 0.31
$D_s^- \rightarrow K_S^0 K^+ \pi^- \pi^-$	21.30 \pm 0.14	21.85 \pm 0.06	21.66 \pm 0.08	22.27 \pm 0.16
$D_s^- \rightarrow \pi^- \pi^- \pi^+$	53.43 \pm 0.34	51.38 \pm 0.15	50.48 \pm 0.21	50.73 \pm 0.42
$D_s^- \rightarrow \pi^- \eta$	44.03 \pm 0.34	43.64 \pm 0.15	43.10 \pm 0.21	43.10 \pm 0.41
$D_s^- \rightarrow \pi^- \eta_{\pi^+ \pi^- \eta \gamma \gamma}$	18.92 \pm 0.13	19.05 \pm 0.06	18.99 \pm 0.08	19.15 \pm 0.13
$D_s^- \rightarrow K^- \pi^+ \pi^-$	48.37 \pm 0.59	47.93 \pm 0.25	47.63 \pm 0.34	47.67 \pm 0.67

TABLE VI. The DT efficiencies (ϵ^{DT}) of $D_s^+ \rightarrow K_S^0 K_L^0 \pi^+$ at $\sqrt{s} =$ (I) 4.128–4.157, (II) 4.178, (III) 4.189–4.219, and (IV) 4.226 GeV. The efficiencies include the sub-resonance decays, and the uncertainties are statistical only.

Tag mode	(II) $\epsilon^{\text{DT}}(\%)$	(II) $\epsilon^{\text{DT}}(\%)$	(III) $\epsilon^{\text{DT}}(\%)$	(IV) $\epsilon^{\text{DT}}(\%)$
$D_s^- \rightarrow K_S^0 K^-$	14.39 \pm 0.39	14.20 \pm 0.17	13.14 \pm 0.20	12.61 \pm 0.33
$D_s^- \rightarrow K^+ K^- \pi^-$	11.61 \pm 0.15	11.28 \pm 0.07	10.70 \pm 0.08	9.92 \pm 0.13
$D_s^- \rightarrow K^+ K^- \pi^-$	5.26 \pm 0.24	5.59 \pm 0.11	5.00 \pm 0.13	4.58 \pm 0.20
$D_s^- \rightarrow K^+ K^- \pi^- \pi^0$	3.74 \pm 0.09	3.79 \pm 0.04	3.65 \pm 0.05	3.43 \pm 0.07
$D_s^- \rightarrow K_S^0 K^- \pi^+ \pi^-$	4.72 \pm 0.28	5.21 \pm 0.13	4.82 \pm 0.16	4.70 \pm 0.25
$D_s^- \rightarrow K_S^0 K^+ \pi^- \pi^-$	5.08 \pm 0.23	5.42 \pm 0.10	5.18 \pm 0.12	4.76 \pm 0.20
$D_s^- \rightarrow \pi^- \pi^- \pi^+$	16.18 \pm 0.40	16.53 \pm 0.18	15.20 \pm 0.21	14.01 \pm 0.34
$D_s^- \rightarrow \pi^- \eta$	13.48 \pm 0.47	13.35 \pm 0.20	12.50 \pm 0.25	12.09 \pm 0.40
$D_s^- \rightarrow \pi^- \eta'$	6.42 \pm 0.32	6.35 \pm 0.14	6.00 \pm 0.17	6.32 \pm 0.29
$D_s^- \rightarrow K^- \pi^- \pi^+$	14.25 \pm 0.49	14.40 \pm 0.22	13.28 \pm 0.26	13.22 \pm 0.43